J Math Chem (2013) 51:465–491
DOI 10.1007/s10910-012-0098-3

ORIGINAL PAPER

Effective GA approach for a direct evaluation of reaction kinetic within EPDM accelerated sulphur crosslinking

G. Milani

Received: 9 August 2012 / Accepted: 21 September 2012 / Published online: 6 October 2012

Abstract A direct genetic algorithm (GA) approach with kinetic base, to provide effective numerical estimates of vulcanization level for EPDM cross-linked with accelerated sulphur is presented. The model requires a preliminary characterization of rubber through standard rheometer tests. A recently presented kinetic exponential model is used as starting point to develop the algorithm proposed. In such a model, three kinetic constants have to be determined by means of a non-linear least-squares curve fitting. The approach proposed circumvents a sometimes inefficient and not convergent non-linear data fitting, disregarding at a first attempt reversion and finding the local minimum of a suitable two-variable error function, to have an estimate of the first two kinetic constants. A comparison between present GA approach and traditional gradient based algorithms is discussed. The last constant, representing reversion is again evaluated through a minimization performed on a single variable error function. The applicability of the approach is immediate and makes the model extremely appealing when fast and reliable estimates of crosslinking density of cured EPDM are required. To show the capabilities of the approach proposed, a comprehensive comparison with both available experimental data and results obtained numerically with a least square exponential model for a real compound at different temperatures is provided.

Keywords Simplified kinetic model · Genetic algorithm (GA) · Sulphur vulcanization · Reversion · Rheometer curve fitting

G. Milani (✉)
Politecnico di Milano, Piazza Leonardo da Vinci 32, 20133 Milan, Italy
e-mail: milani@stru.polimi.it; gabriele.milani@polimi.it

1 Introduction

A good vulcanization, macroscopically intended as the mechanical performance of an item after curing, is obtained when the level of reticulation reached point by point by a rubber specimen subjected to prescribed temperature and cure time conditions is optimal. The most straightforward way to predict such vulcanization degree is the utilization of suitable theoretical or numerical models. For peroxidic curing, literature is wide, see e.g. [1–7], whereas for sulphur vulcanization little references are at disposal, because of the extremely intricate crosslink chemistry, associated to multiple reactions occurring in series and parallel. At present, while the utilization of sulphur is quantitatively predominant for economic reasons, comprehensive models seem still a few, despite the technology goes back to Goodyear [8–11].

The present paper may be regarded as a further improvement in the efficiency of a numerical approach developed in the last few years by the Author [12–16] both from a heuristic and kinetic standpoint, to predict the vulcanization degree of rubber cured with sulphur.

From a mathematical point of view, the model relies into a second order non homogeneous differential equation with constant coefficients, where a closed form solution exists. The function representing the final polymer crosslink density is expressed by the sum of three exponential functions, all depending on both curing time and three reaction kinetic constants, the latter further depending on curing temperature.

An evaluation of such kinetic constants has been attempted through experimental data fitting on the so-called rheometer test [17–19]. The fundamental importance of this test for the experimental characterization of crosslinking has been acknowledged in the recent past by many authors, especially Poh and co-workers [20–24]. Such standard test is usually performed maintaining a small rubber cylindrical specimen inside a chamber at fixed vulcanization temperature, where a metallic disc oscillates. Torque resistance to oscillation is registered at increasing exposition times and plotted in a so-called rheometer chart or cure curve, thus giving indirect macroscopic information on rubber reticulation kinetics at fixed temperature. Typically, both natural and synthetic rubber exhibit a decrease in the initial part of the test, followed by a sudden increase at approximately 1/3 of time needed to complete the test (scorch time). In several cases, torque decreases near the end of the experimentation, such behavior being commonly associated to reversion.

Reversion occurs quite frequently in practice and consists in a remarkable decrease of rubber vulcanized properties at the end of the curing process. Chen and co-workers [25] have shown that this phenomenon seems to appear when two reactions are competing during vulcanization. Reversion is often associated with high-temperature curing. In agreement with the studies conducted by Loo [26], it can be stated that, generally, when the cure temperature rises, the crosslink density drops, thus increasing the degree of reversion. Morrison and Porter [27] confirmed that the observed reduction in vulcanizate properties is caused by two reactions proceeding in parallel, i.e. de-sulphuration and decomposition, see Table 1.

A single compound has its own characteristic cure curve at fixed temperature, which fully describes from a macroscopic point of view the blend reticulation. A change in both accelerators molar ratios and temperature room changes the cure curve.

Table 1 Products and schematic reaction mechanisms of accelerated sulphur vulcanization of poly-diene and EPDM elastomers

Reaction ID	Compounds	Process/reaction	Kinetic constant	Model constants
NA	$S_8 + \text{accelerators} + \text{ZnO} + \text{stearicacid} \rightarrow$ soluble sulphurate zinc complex (A) + polydiene elastomers (P)	Mechanical mixing by open roll mill, internal mixers and/or extruders at T $< 100\,^{\circ}\text{C}$	NA	NA
(a)	$P + A \overset{K_1}{\rightarrow} P_1^*$	Allylic substitution	K_1	K_1
(b)	$P_1^* \overset{K_2}{\rightarrow} P$	Disproportionation	K_2	K_2
(c)	$P_v \overset{K_3}{\rightarrow} Q_x$	Oxidation	K_3	$\tilde{K}$
(d)	$P_v \overset{K_4}{\rightarrow} D_e$	De-sulphuration	K_4	
(e)	$P_v \overset{K_5}{\rightarrow} P_{v_f}$	De-vulcanization	K_5	

Milani and Milani [14,15] estimated numerically reticulation kinetic constants by means of non-linear least squares performed either on a system of first order differential equations [28] or on a single second order differential equation [14]. Such approach has been recently superseded by the same authors in [16], and simplified closed form formulas have been provided to avoid tedious and sometimes inefficient numerical procedures based on non-linear programming routines.

In this paper, a new very efficient numerical procedure is proposed to determine numerically kinetic constants. The model moves its steps from the simplified formula proposed in [16] for vulcanization without reversion. Such model is a good base to determine the first two kinetic constants, say K_1 and K_2, whereas the third ($\tilde{K}$, which represents the amount of reversion) is a-posteriori evaluated once the first two kinetic constants are known.

In absence of reversion, it is shown that the function representing the relative error between experimental and numerical crosslinking density at each sampled point during the vulcanization process is a two variables function, being independent variables K_1 and K_2, symmetric with respect to K_1 and K_2.

It is shown how such cumulative error function has two symmetric minimum points, providing the best fitting values of K_1 and K_2. Such minimum may be evaluated both by means of either standard gradient based approaches [29,30], or Genetic Algorithms (GAs) [31–33], which seem more indicated for such specific problem where the objective function is the sum of relative errors between sampled and predicted values. The last constant, representing reversion is again evaluated through a minimization performed on a single variable error function. The applicability of the approach is immediate and makes the model extremely appealing when fast and reliable esti-

mates of crosslinking density of cured EPDM are required. To show the capabilities of the approach proposed, a comprehensive comparison with both available experimental data and results obtained numerically with a least square exponential model for a real compound at different temperatures is provided. The numerical example shows a considerable speed-up of computational time when the GA proposed is used instead of gradient based methods.

2 Chemistry of vulcanization

Pioneering analytical contributions regarding vulcanization with sulphur, almost always, may be regarded as simplified approaches allowing a crude estimation of the final crosslinking degree of small specimens, under controlled time and temperature conditions, see e.g. [34–39]. Conceived essentially for natural rubber, they basically rely into simplified kinetic models enforced to follow differential equations similar to those used for peroxidic curing, basing on an experimental data fitting performed on rheometer charts, to deduce kinetic constants.

To circumvent limitations of such models in the application of EPDM rubber, the mechanisms at the base of vulcanization for such material should be properly considered.

For EPDM rubber, the commonly accepted basic reactions involved—see also [14, 39,40]—are summarized in Table 1. In Table 1, P and A are the polymer (EPDM) and soluble sulphureted zinc complex (S_8 + accelerators + ZnO + stearic acid) respectively, P_1^* is the pendent sulfur (crosslink precursor), P_v is the reticulated EPDM, P_{v_f} is the matured cross-link, Q_x is the oxidation product, D_e represents diaryl-disulphide and $K_{1,\ldots,5}$ are kinetic reaction constants. Here it is worth emphasizing that $K_{1,\ldots,5}$ are temperature dependent quantities, hence they rigorously should be indicated as $K_{1,\ldots,5}(T)$, where T is the absolute temperature. In what follows, for the sake of simplicity, the temperature dependence will be left out.

Reaction (a) in Table 1 represents the allylic substitution, reaction (b) is the disproportionation, whereas reactions (c) (d) and (e) occurring in parallel are respectively the oxidation, the de-sulphuration and the de-vulcanization.

A purely phenomenological interpretation of sulphur vulcanization has been recently proposed by the Author in [12,13], respectively in absence and presence of reversion. In both models a curve fitting is proposed, which approximates the rheometer chart by means of two parabolas and one hyperbola. In case of reversion, the hyperbola is rotated with respect to coordinate axes. While the application of such model is very straightforward for practical purposes, the absence of a kinetic base does not permit to generalize the models to any vulcanization temperature directly from the numerical model and a huge amount of experimental data is needed.

To supersede such limitation, very recently, in [14,15] a relatively simple numerical model basing on actual reaction kinetics of Table 1 has been proposed, where rubber crosslinking density during vulcanization may be found solving a non-homogeneous second order differential equation with unknown constant coefficients. The approach is fully based on reaction kinetic characterizing EPDM sulphur curing. Independent unknown coefficients are only three, and may be regarded as a combination of kinetic

constants associated to partial reactions occurring during vulcanization, Table 1. Milani and Milani [14,15] proposed to estimate numerically independent coefficients through a data fitting on experimental rheometer curves available for a given compound, thus indirectly evaluating the crosslinking degree from a macroscopic test. The approach is mathematically rather simple, but has the drawback of requiring a material identification through non-linear least square routines or large scale Genetic Algorithms with three independent variables.

Available software is usually stable, but sometimes may be tedious in the calibration of code options, as for instance the choice of the initial iteration values for the independent variables to identify. To circumvent such intrinsic limitation of the procedure, and to make it immediately applicable by manufacturers, in the present paper a new approach, which still bases on the original model proposed in [14,15], but allows a kinetic characterization of the parameters by means of the minimization of simple functions, is presented.

The first improvement relies into the approximation of the numerical cure curve provided in [14,15] with a two-variable function without reversion.

Such function, depending exclusively on K_1 and K_2 kinetic constants (here regarded as problem unknowns), is used to evaluate the cumulative relative error e between numerical and experimental data. e is still a two-variable function, symmetric around the first quadrant bisecting line and admitting two symmetric minimum points in correspondence of K_1 and K_2 values allowing an optimal fitting of the experimental data.

The second improvement relies into the determination of e minimum points by means of a non-standard Genetic Algorithm

The improved model is tested at three different temperatures on a real EPDM compound, exhibiting remarkable reversion over 180 °C. Rheometer charts so evaluated are compared with curves provided by the model proposed in [14,15], available experimental data and a simplified approached without reversion. Finally kinetic constants so obtained are again compared with those provided by an approach based on linear least square fitting of the second order non homogeneous differential equation by Milani and Milani [14,15].

Within the limits of the benchmark discussed, results are in excellent agreement with existing literature, exhibiting errors in the estimation of kinetic constants not exceeding 5 %, meaning that the direct procedure presented may represent a valuable tool for all manufactures interested in a fast prediction of the level of crosslinking of EPDM cured with sulphur.

3 GA kinetic numerical model

In [15], an exponential model to interpret, from a kinetic point of view, vulcanization of EPDM cured with accelerated sulphur was proposed. The model is quite appealing, because allows for a mathematical estimate of EPDM crosslinking density. However, kinetic constants calibration has to be done on rheometer data through best fitting and with the subsequent utilization of non-linear least square routines. To supersede such major limitation exhibited by [15] model, in [16] a non-standard alternative procedure is proposed. Essentially, several restrictive hypotheses on the free-variables are

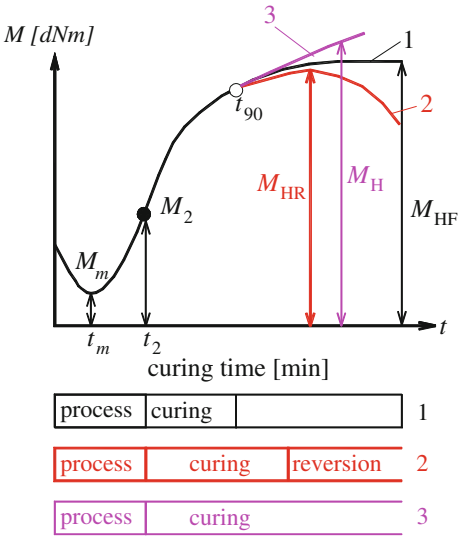

Fig. 1 Typical experimental behaviour of a rubber compound during rheometer test

assumed, disregarding suitably the contribution of some terms within the formulation, and providing closed form formulas for a direct, despite approximate, evaluation of the constants.

Here, a further improved approach is proposed, which avoids the assumption of questionable hypotheses on the free-variables involved.

To make the model fully clear, the main features related to the exponential model proposed in [14,15] are hereafter briefly recalled. As a matter of fact, the worldwide recognized standard experimental test to evaluate macroscopically the vulcanization characteristics of vulcanizable rubber compounds is the so-called curometer test [34].

In one version of such a device (oscillating disc rheometer) the rubber sample is enclosed within a heated chamber. Vulcanization is measured by the increase in the torque required to maintain a fixed amplitude of oscillation at a given temperature. The torque is thus roughly proportional to reticulation. The torque is plotted against time to give a so-called rheometer chart, rheograph or cure curve, which exhibits a number of features used to compare cure.

In a rheometer chart, the resistance to oscillation (torque) is measured and recorded as a function of time, as in Fig. 1. In practice, three different cases can occur: (1) the curve reaches a maximum asymptotically, (2) the curve reaches a maximum and then decreases (reversion) and (3) the curve increases monotonically after the scorch point t_2. In Fig. 1 the so called t_{90} point is also represented. It is defined as the time to achieve 90 % cure. The second case is encountered very frequently in practice, because reversion is a distinguishing characteristic of sulphur curing (Table 1), especially at high temperatures.

The numerical algorithm proposed is based on the experimental use of rheometers at different temperatures, which allows collecting a suitable database of experimental data regarding cure curves at increasing temperatures and their successive interpolation by means of a simple kinetic mathematical formulation.

At present, the knowledge regarding the chemistry of accelerated sulphur vulcanization seems a bit fragmented; some useful experimental data are available from Poh and co-workers [20–24], who observed a marked relation among scorch time, amount of activators used and rheometer temperatures. Unfortunately, numerical and/or theoretical models in this field are a few and mainly based on phenomenological considerations [37,39].

At present, it is commonly accepted that chemical reactions occurring during sulfur vulcanization, Table 1, obey the following rate equations:

$$\begin{aligned}
\frac{dP}{dt} &= -K_1 A P \\
\frac{dP_v}{dt} &= K_2 P_1^* - K_3 Q_x - K_4 D_e - K_5 P_{v_f} \\
\frac{dQ_x}{dt} &= K_3 P_v \\
\frac{dD_e}{dt} &= K_4 P_v \\
\frac{dP_{v_f}}{dt} &= K_5 P_v
\end{aligned} \tag{1}$$

By means of the so called xyz method, independent variables may be established.

From stoichiometry of the reaction, it can be argued that:

$$\begin{aligned}
A &= A_0 - x \\
P &= P_0 - x \\
P_1^* &= x - y = (P_0 - P) - y = (P_0 - P) - \left(P_v + Q_x + D_e + P_{v_f}\right) \\
P_v &= y - z - q - r \\
Q_x &= z \\
D_e &= q \\
P_{v_f} &= r
\end{aligned} \tag{2}$$

where $x = P(t)$, $y = P_v(t)$, $z = Q_x(t)$, $q = D_e(t)$, $r = P_{v_f}(t)$ identify independent variables, P_0 and A_0 are the initial molar concentrations of polymer and curing agent (or better the soluble sulphur agent zinc complex, i.e. S_8+Accelerators+ZnO+Stearic acid) respectively. Typically they are known production parameters (they may obviously vary from case to case) and they are obtained mixing all the components in an internal mixed before vulcanization.

The aim of the approach is to provide an analytical expression for vulcanized rubber, i.e. concentration of $P_v(t)$ with respect to time.

From (1) and (2), the following set of differential equations is deduced:

$$(a) \quad \frac{dP}{dt} = -K_1 A P$$

$$(b) \quad \frac{dP_v}{dt} = K_2 P_1^* - K_3 Q_x - K_4 D_e - K_5 P_{v_f}$$

$$= K_2\left[(P_0 - P) - \left(P_v + Q_x + D_e + P_{v_f}\right)\right] - K_3 Q_x - K_4 D_e - K_5 P_{v_f}$$

$$(c)\quad \frac{dQ_x}{dt} = K_3 P_v$$

$$(d)\quad \frac{dD_e}{dt} = K_4 P_v$$

$$(e)\quad \frac{dP_{v_f}}{dt} = K_5 P_v \tag{3}$$

Obviously the first order differential equation system (3) can be solved using a standard Runge-Kutta numerical approach [28,29]. However, such a procedure, when coupled with a non-linear least square algorithm (as in the present case) may become very tedious to be performed (especially for stiff problems) and in some cases may fail to converge during experimental data fitting. Here, an alternative procedure based on the derivation of a single differential equation is adopted.

Milani and Milani in [13,14] deduced from (3) the following single second order non homogeneous differential equation with constant coefficients:

$$\frac{d^2 P_v}{dt^2} + K_2 \frac{dP_v}{dt} + \tilde{K}^2 P_v = -K_2 \frac{dP}{dt} = \frac{K_1 K_2 P_0^2}{(P_0 K_1 t + 1)^2} \tag{4}$$

Equation (4) admits the following closed form solution in the normalized concentration of vulcanized polymer $P_v(t)$:

$$\begin{aligned}
&P_v(t) = C_1 e^{(\alpha+\beta)t} + C_2 e^{(\alpha-\beta)t} + \rho e^{-K_1 P_0 t} \\
&\begin{cases}
C_2 = \rho\left(-\frac{K_1 P_0}{2\beta} - \frac{\alpha}{2\beta} - \frac{1}{2}\right) \\
C_1 = \rho\left(\frac{K_1 P_0}{2\beta} + \frac{\alpha}{2\beta} - \frac{1}{2}\right) \\
\rho = K_1 K_2 P_0^2\left[(K_1 P_0)^2 - K_2 (K_1 P_0) + \tilde{K}^2\right]^{-1} \\
\alpha = -\frac{K_2}{2} \\
\beta = \sqrt{(K_2/2)^2 - \tilde{K}^2} \\
\tilde{K}^2 = \tilde{K}^2 = K_2 (K_3 + K_4 + K_5) + K_3^2 + K_4^2 + K_5^2
\end{cases}
\end{aligned} \tag{5}$$

Kinetic constants to determine are only three, namely K_1, K_2 and $\tilde{K}^2$.

The most straightforward method to numerically estimate such kinetic constants is that followed in [15], relying into a experimental cure-curve data fitting, performed normalizing experimental data at peak to P_0 and translating the initial rotation resistance to zero, as suggested by Ding and Leonov [34].

In [15], K_1, K_2 and $\tilde{K}^2$ variables are found through a standard nonlinear least square routine. To make the notation easier, we consider in the following as one of the free variables to optimize $\tilde{K}_1$ instead of K_1, having defined $\tilde{K}_1 = P_0 K_1$.

A simplified but quite effective approach has been very recently proposed in [16], where iterative algorithms on a less complex version of Eq. (5) have been used to separately evaluate constants. The approach has been tested on real scale examples, showing good stability and errors generally not exceeding 5 %.

Here the research is further put forward and a new fully numerical procedure is proposed to evaluate exactly unknown kinetic constants.

The advantage with respect to [16] procedure is that in this case the evaluation of K_1, K_2 and $\tilde{K}^2$ occurs utilizing the actual error functions evaluated on experimental data, as it will be shown hereafter.

In the common case of compounds with little or no reversion, $\tilde{K}$ kinetic constant is assumed reasonably equal to zero, and hence Eq. (5) simplifies as follows, being $|\alpha| \approx |\beta| \approx K_2/2$ and $\rho = P_0 K_2/(\tilde{K}_1 - K_2)$:

$$\begin{aligned} P_v(t) &= C_1 - \rho\frac{\tilde{K}_1}{K_2}e^{-K_2 t} + \rho e^{-\tilde{K}_1 t} = \rho\left(\frac{\tilde{K}_1}{2\beta} - 1\right) - \rho\frac{\tilde{K}_1}{K_2}e^{-K_2 t} + \rho e^{-\tilde{K}_1 t} \\ &= \frac{P_0 K_2}{\left(\tilde{K}_1 - K_2\right)}\left(\frac{\tilde{K}_1}{K_2} - 1 + e^{-\tilde{K}_1 t} - \frac{\tilde{K}_1}{K_2}e^{-K_2 t}\right) \\ \Rightarrow P_v(t) &= P_0\left[1 + \frac{K_2}{\left(\tilde{K}_1 - K_2\right)}e^{-\tilde{K}_1 t} - \frac{\tilde{K}_1}{\left(\tilde{K}_1 - K_2\right)}e^{-K_2 t}\right] \end{aligned} \tag{6}$$

Assuming to have at disposal values of the normalized torque (either experimental or derived from the aforementioned exponential numerical model) at increasing instants t_i, hereafter called $P_{\exp}(t_i)$, it is possible to evaluate the total relative error function as:

$$\begin{aligned} e\left(\tilde{K}_1, K_2\right) &= \sum_{i=1}^{N_{sam}} \frac{\left|P_{\exp}(t_i) - P_v(t)\right|}{P_{\exp}(t_i)} \\ &= \sum_{i=1}^{N_{sam}} \frac{\left|P_{\exp}(t_i) - P_0\left[1 + \frac{K_2}{\left(\tilde{K}_1 - K_2\right)}e^{-\tilde{K}_1 t_i} - \frac{\tilde{K}_1}{\left(\tilde{K}_1 - K_2\right)}e^{-K_2 t_i}\right]\right|}{P_{\exp}(t_i)} \end{aligned} \tag{7}$$

where N_{sam} is the number of sampled instants where the torque is known.

Equation (7) is a function depending on two variables ($\tilde{K}_1$ and K_2) which is not analytically known, but may be easily plotted point by point with a regular mesh-grid for $\tilde{K}_1$ and K_2.

A common procedure, used as comparison in the paper, to find local minima for function (7) within an unconstrained minimization scheme is the well-known BFGS Quasi-Newton method with cubic line search procedure [30]. Usually, the BFGS formula for updating the approximation of the Hessian matrix is used.

However, since function (7) is the sum of single contributions on discrete sampled points, it appears quite beneficial the utilization of a Generic Algorithm instead of traditional optimization, requiring a GA only the iterated evaluation of the objective function on specific sampled points.

Here it is worth noting that function (7) is symmetric in $\tilde{K}_1$ and K_2, i.e. $e_{\%}(\tilde{K}_1, K_2) = e_{\%}(K_2, \tilde{K}_1)$.

This implies that the minimum of the total relative error will be achieved at least in correspondence of two points, placed symmetrically with respect to the bisector axis.

Values of $\tilde{K}_1$ and K_2 which minimize $e_{\%}(\tilde{K}_1, K_2)$ are those which allow to fit as close as possible experimental data. To find such points it would be necessary to study first of all if stationary points for (7) exist. At this aim, the gradient of (7) may be written as follows:

$$
\begin{aligned}
e_{\%}\left(\tilde{K}_1, K_2\right) &= \sum_{i=1}^{N_{sam}} \frac{\left|P_{\exp}(t_i) - P_v(t)\right|}{P_{\exp}(t_i)} \\
&= \sum_{i=1}^{N_{sam}} \frac{\left|P_{\exp}(t_i) - P_0\left[1 + \frac{K_2}{\left(\tilde{K}_1 - K_2\right)} e^{-\tilde{K}_1 t_i} - \frac{\tilde{K}_1}{\left(\tilde{K}_1 - K_2\right)} e^{-K_2 t_i}\right]\right|}{P_{\exp}(t_i)} \\
\begin{bmatrix} \frac{\partial e\left(\tilde{K}_1, K_2\right)}{\partial \tilde{K}_1} \\ \frac{\partial e\left(\tilde{K}_1, K_2\right)}{\partial K_2} \end{bmatrix} &= \begin{bmatrix} \frac{P_0}{P_{\exp}(t_i)} \sum_{i=1}^{N_{sam}} \left| -\frac{K_2 e^{-\tilde{K}_1 t_i}}{\left(\tilde{K}_1 - K_2\right)^2} - \frac{t_i K_2 e^{-\tilde{K}_1 t_i}}{\left(\tilde{K}_1 - K_2\right)} + \frac{K_1 e^{-K_2 t_i}}{\left(\tilde{K}_1 - K_2\right)^2} - \frac{e^{-K_2 t_i}}{\left(\tilde{K}_1 - K_2\right)} \right| \\ \frac{P_0}{P_{\exp}(t_i)} \sum_{i=1}^{N_{sam}} \left| -\frac{\tilde{K}_1 e^{-\tilde{K}_2 t_i}}{\left(\tilde{K}_1 - K_2\right)^2} + \frac{t_i \tilde{K}_1 e^{-\tilde{K}_2 t_i}}{\left(\tilde{K}_1 - K_2\right)} + \frac{\tilde{K}_2 e^{-K_1 t_i}}{\left(\tilde{K}_1 - K_2\right)^2} + \frac{e^{-\tilde{K}_1 t_i}}{\left(\tilde{K}_1 - K_2\right)} \right| \end{bmatrix}
\end{aligned}
\tag{8}
$$

To evaluate stationary point from (7) and the typology of stationarity by means of the Hessian is not an easy task. An alternative to solve the non-liner system of Eq. (8) numerically is the following. Let's assume as $f(\tilde{K}_1, K_2) = \frac{\partial e(\tilde{K}_1, K_2)}{\partial \tilde{K}_1} = 0$ and $g(\tilde{K}_1, K_2) = \frac{\partial e(\tilde{K}_1, K_2)}{\partial \tilde{K}_2} = 0$. It is possible to plot $f(\tilde{K}_1, K_2) = 0$ assuming a priori a value for K_2, say $\bar{K}_2$, and find the zero of the single variable function $f(\tilde{K}_1, \bar{K}_2)$ with a standard Newton approach. The same may be repeated for $g(\tilde{K}_1, K_2) = 0$.

The point of intersection of the two implicit functions will obviously represent the minimum point for (7).

Having defined with $e_{\%}^{\min}$ the minimum total relative error corresponding to point $(\tilde{K}_1^{\min}, K_2^{\min})$, the symmetric point $(K_2^{\min}, \tilde{K}_1^{\min})$ will be associated to the same minimum error. For physical reasons related to reaction velocity we implicitly assumed the solution point $(\tilde{K}_1^{\min}, K_2^{\min})$ as effective solution for both the traditional optimization and GA problems under consideration.

When $(K_2^{\min}, \tilde{K}_1^{\min})$ values are know either from classic optimization strategy or GAs, the third kinetic constant may be evaluated again from an error function, say e_2, but in this case evaluated using (5). To summarize, function e_2 is the following:

$$
\begin{aligned}
P_v(t) &= \rho\left(\frac{K_1 P_0}{2\beta} + \frac{\alpha}{2\beta} - \frac{1}{2}\right) e^{(\alpha+\beta)t} + \left(-\frac{K_1 P_0}{2\beta} - \frac{\alpha}{2\beta} - \frac{1}{2}\right) e^{(\alpha-\beta)t} + \rho e^{-K_1 P_0 t} \\
\rho &= K_1 K_2 P_0^2 \left[(K_1 P_0)^2 - K_2 (K_1 P_0) + \tilde{K}^2\right]^{-1}
\end{aligned}
$$

$$\alpha = -\frac{K_2}{2}$$

$$\beta = \sqrt{(K_2/2)^2 - \tilde{K}^2}$$

$$e_2\left(\tilde{K}\right) = \sum_{i=1}^{N_{sam}} \frac{\left|P_{\exp}(t_i) - P_v(t)\right|}{P_{\exp}(t_i)}$$

$$= \sum_{i=1}^{N_{sam}} \frac{\left|P_{\exp}(t_i) - \rho\left(\frac{K_1 P_0}{2\beta} + \frac{\alpha}{2\beta} - \frac{1}{2}\right) e^{(\alpha+\beta)t} + \left(-\frac{K_1 P_0}{2\beta} - \frac{\alpha}{2\beta} - \frac{1}{2}\right) e^{(\alpha-\beta)t} + \rho e^{-K_1 P_0 t}\right|}{P_{\exp}(t_i)} \tag{9}$$

3.1 The genetic algorithm proposed

The advantage of using a GA instead of traditional methods is very straightforward for the case under consideration and is essentially related to the fact that total relative error functions are evaluated on a finite number of (experimental) points and are obtained through a sum operator.

Hence, it is expected that the evaluation of kinetic constants K_1, K_2 and $\tilde{K}^2$ is easier and requires less time to be performed using genetic schemes [31–33], where only repeated computations of the values assumed by the objective function on a limited number of sampled points is needed. In addition, the theoretical simplicity of the GAs makes them quite immediate to be implemented in a computer code.

Genetic algorithms belong the large family of meta-heuristic methods, which result rather suited for solving both constrained and unconstrained optimization problems basing on natural selection, the process that drives biological evolution. A genetic algorithm repeatedly modifies a population of individual solutions. At each step, GA individuals are selected randomly from the current population to be parents and utilized to produce the children for the next generation. Over successive generations, the population "evolves" toward an optimal solution. Typically genetic algorithms are used to solve a variety of optimization problems that are not well suited for standard optimization algorithms, including problems in which the objective function is discontinuous, non-differentiable, stochastic, or highly nonlinear.

The kernel of the GA proposed has been already successfully applied to a variety of different chemical problems (see e.g. [14,41]) and relies into a set of both standard genetic operations (reproduction, crossover and mutation) and non-standard procedures, such as zooming and elitist strategy (see [41] for further details on this issue).

Hereafter, a very concise overview of the procedures used is summarized for the sake of conciseness: the reader interested to details of the non-standard GA approach proposed is referred to [14,41].

"Selection" rules select a part of individuals contributing as parents to the population at the next generation. "Crossover" combines two parents to form children for the next generation, whereas "mutation" applies random changes to individual parents to form children.

"Zooming" and the "elitist tool" are strictly related and consist in sub-dividing the initial population into two groups, say:

$$\bar{\mathbf{x}} = \{\bar{x}_i : i = 1, \ldots, N_{elit} | x_i \text{ admissible}\}$$
$$\mathbf{y} = \mathbf{x} - \bar{\mathbf{x}} = \{y_i : i = 1 :, \ldots, N_{ind} - N_{elit}\} \tag{10}$$

where N_{elit} is the number of "elite" individuals, i.e. points with sufficiently good fitness, N_{ind} is the total number of individuals and $\mathbf{x}$ is the individuals vector.

The core of the so called "zooming strategy" consists in collecting at each iteration the individuals with higher fitness into an "elite" sub-population $\bar{\mathbf{x}}$ (with user defined dimension N_{elit}). Then, for each individual belonging to group $\bar{\mathbf{x}}$, only mutation (with high probability) is applied in order to improve individuals fitness. Two different mutation algorithms are utilized, differing only on the number of cells of each individual involved by the mutation process.

Subsequently, an elitist strategy preserves the original individual if mutation results in a reduction of individual fitness, whereas zooming technique restricts search domain, so improving in any case convergence rate.

From a practical point of view, zooming has to be a priori set by the user by means of the so called zooming percentage $z_{\%}$ defined as the percentage ratio between $\mathbf{x}$ initial population and $\bar{\mathbf{x}}$ sub-population dimension, i.e.:

$$z_{\%} = \frac{N_{elit}}{N_{ind}} 100 \tag{11}$$

Even if the zooming percentage is taken constant in this paper, $z_{\%}$ can be reduced if necessary at user's desire, passing from the ith iteration to the successive, following the exponential reduction proposed by Milani and Milani in [41].

Mutation is applied with high probability directly on existing individuals. As already pointed out, two types of mutation are used (here denoted as 1st and 2nd type).

1st type is the classic mutation and is applied both on $\bar{\mathbf{x}}$ and $\mathbf{y}$ individuals. For each individual $\bar{x}_i$ (or y_i) it works stochastically on all the chromosomes (i.e. changing at random one of the individual columns from 1 to N_{bit}). The procedure is repeated once on N_{mut} different individuals. Obviously, first type mutation results in a new individual in which only one of the optimization independent variables, after chromosomes decoding, results changed with respect to the original individual.

2nd type mutation is applied only to $\bar{\mathbf{x}}$ individuals, in order to obtain a further improvement of their fitness. It works analogously to the first type algorithm, with the only difference that it changes, for the individual subjected to mutation, a chromosome belonging to $\tilde{K}_1$ and K_2 respectively. Thus, the resulting individual after chromosomes decoding is different from the original one for all the kinetic constants. The procedure is repeated on N_{mut2} individuals. Both N_{mut} first type mutations and N_{mut2} second type mutations are user defined.

The final result of the application of both first and second type mutation is a new admissible individual $\bar{x}_{iM}$ with different fitness with respect to $\bar{x}_i$. If $\bar{x}_{iM}$ fitness is higher than that of the original individual (note that the check is executed at each N_{mut} iteration), $\bar{x}_i$ is overwritten with $\bar{x}_{iM}$. All the fitting procedure is handled within the Matlab software by means of non standard routines implemented at this aim by the author.

To solve optimization problem (8), each individual is identified by a pair $(\tilde{K}_1^i, K_2^i)$ and encoded into binary strings. Since individuals are stored as a sequence of two real positive numbers, their encoding by means of binary strings results particularly easy. In this way, the genotypes (chromosome values) can be uniquely mapped onto the decision variable (phenotypic) domain. In a standard GA procedure, the use of Gray coding is necessary to avoid a hidden representational bias in conventional binary representation as the Hamming distance between adjacent values is constant (see Holstien [32] and Haupt and Haupt [33]).

Within the GA scheme, also a limitation in form of linear inequalities is provided, to assure that $K_2^i < \tilde{K}_1^i$ and $\tilde{K}_1^i, K_2^i > 0$. Such a standard constraints obviously are accounted for both within mutation and crossover operations, assuming as inadmissible children not respecting the aforementioned inequalities.

The author compared the performance of standard optimization approaches [both unconstrained optimization (7) and non-linear system of Eq. (8)] to find $(\tilde{K}_1^i, K_2^i)$ pair which minimizes e function to GA performance, as it will be shown in the numerical analyses reported hereafter, finding a substantial advantage in the use of GAs.

Genetic Algorithms may be also used to find kinetic constant $\tilde{K}$ (or equivalently $\tilde{K}^2$), minimizing error function $e_2(\tilde{K})$ in Eq. (9), but in this case the utilization of a standard Newton approach appears still enough efficient, being e_2 a single variable function.

4 Numerical applications

The efficiency of the GA approach proposed is tested on an EPDM blend with experimental data available from the literature [18]. Experimental data basically rely into cure curves performed at three different temperatures, namely 160, 180 and 200 °C. Three different temperatures are considered, in order to have information on the variability of kinetic constants with respect to temperature.

To perform a numerical optimization of the kinetic model proposed, experimental cure values are normalized dividing each point of the curve by the maximum torque values, so that experimental data are always within the range 0–1, and cutting the first part of the curves before the scorch time. Indeed, the first descending branch of the rheometer chart is the result of a typical behavior of unvulcanized rubber connected to viscosity, which cannot be reproduced with kinetic models.

Rheometer charts were obtained by mean of a Monsanto Oscillating Disc Rheometer ODR with an arc deflexion of 3°. The compound exhibits a medium-high level of unsaturation: it is therefore quite indicated to check the predictivity of the model proposed, because unsaturation always corresponds to remarkable reversion. It is worth remembering that a reversion condition is the most difficult characteristic to reproduce with any numerical model and it is hence a good benchmark to test the reliability of the present approach. The composition of the EPDM hereafter considered is schematically summarized in Table 2.

In Fig. 2, a comparison among cure curves provided by the present approach, alternative numerical models and experimental results is sketched for a temperature equal to 160 °C.

Table 2 Experimental data set rubber composition

Polymer type used	DUTRAL 4334	
% of Propylene content by wt	27	
% ENB by wt	4.7	
% oil by wt	30	
Formulation for white items	Description	in phr
Polymer	Dutral 4334	140
Zinc oxide	Activator	5
Stearic acid	Co-agent	3
Clay	Filler	400
Titanium bioxide	Co-agent whitener	15
Paraffinic oil	Wax additive	40
Sulphur	Vulcanization agent	2
TMTD	Accelerator	2
Tetramethylthiuram disulfide		
MBT2	Acceleretor	2
Mercaptobenzothiazole		
Characteristics of the compound		
ML(1+4)100 °C	67	
ODR at 180 °C	t_2 1'06"	
	t_{90} 5'30"	
Characteristics of the vulcanized compound		
Tensile strength Kg/cm^2	80	
Elongation at break %	600	
Hardness Shore A	74	

The continuous thick blue curve is the full experimental curve obtained by ODR tests, whereas the continuous line with diamond symbols is the representation, in the normalized rheometer chart, of Eq. (6), i.e. the model without reversion. Dashed curve represents Eq. (5) where kinetic constants K_1, K_2 and $\tilde{K}$ are evaluated using the present GA approach. Green thin line with green diamonds the same Eq. (5) where kinetic constants are obtained with a non-linear least squares routine, as suggested in [14,15]. As it is possible to notice, the agreement among all models is almost perfect, within all the time range inspected. Even Eq. (6), which is a theoretical model without reversion, fits very well experimental data. This is not surprising, because very little or no reversion is expected at low curing temperatures. GA and least-squares approaches provide almost identical results, as also confirmed by the very small difference among kinematic constants values, see Table 3.

In Fig. 3, error function (7) is graphically represented in the $\tilde{K}_1 - K_2$ domain, with optimization points found using a traditional gradient approach (a, b) and the present GA procedure (c, d). Data are reported both using a 3D representation and in the $\tilde{K}_1 - K_2$ plane, for the sake of clearness.

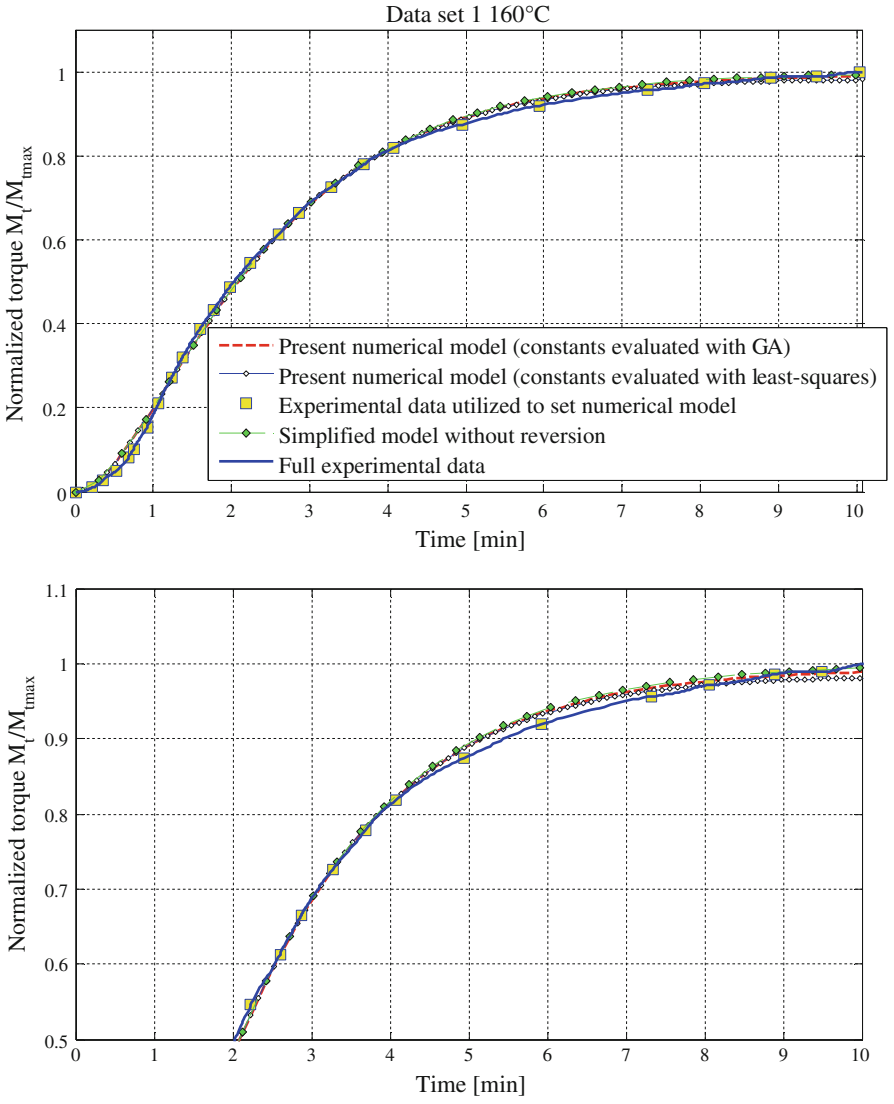

Fig. 2 Experimental data set at 160 °C. Comparison between numerical and experimental curing time-normalized torque (crosslinking density) curves. *Top* entire curve. *Bottom* detail

Graphics clearly show that both gradient and GA approach reach the same optimal solution, but with a substantial advantage for GA, which seems to correctly optimize after very few iterations, as also shown by the best fitness function evaluation reported in Fig. 4.

Once $\tilde{K}_1$, K_2 are estimated with either traditional or heuristic approaches, the evaluation of $\tilde{K}$ is very straightforward finding zeros of Eq. (9). A representation at 160 °C of error function e_2, with the indication of the optimal value for $\tilde{K}$ is provided in Fig. 5.

Table 3 Experimental data set

Kinetic constant [1/sec]	Non-linear least-squares	Simplified method [16]	Present direct model	% error (1)	% error (2)
160 °C					
K_1	0.5671	0.5718	0.5599	1.27	2.08
K_2	1.2567	1.2418	1.2633	−0.52	−1.73
$\tilde{K}$	0.0492	0.0477	0.04800	2.44	−0.63
180 °C					
K_1	0.8903	0.9101	0.8633	3.03	5.14
K_2	2.5501	2.4374	2.6335	−3.27	−8.04
$\tilde{K}$	0.1610	0.1578	0.1591	1.18	−0.82
200 °C					
K_1	1.8106	1.7469	1.7061	5.77	2.33
K_2	7.5407	7.9126	8.078	−7.12	−2.09
$\tilde{K}$	0.5702	0.5839	0.5700	0.03	2.38

Comparison between kinetic constants evaluated by means of the exponential model and the simplified direct model
(1) With least-squares
(2) With simplified method

Having at disposal $\tilde{K}_1$, K_2 and $\tilde{K}$ from the numerical procedure proposed, Eq. (5) may be used directly to fit experimental data with the exponential model, with a direct visual comparison on the normalized cure curves, Fig. 2.

In Table 3, a comparison among kinetic constants provided by least squares fitting [14–16] simplified direct method procedure and present GA approach is summarized. The agreement is very satisfactory, with percentage errors not exceeding 5 % in the most unfavourable case, a result which seems very satisfactory having in mind the practical application of the model proposed.

In Fig. 6, a graphical representation of the procedure used to evaluate $\tilde{K}_1$ and K_2 from the non-linear system of Eq. (8) is provided. In particular, in Fig. 7a, implicit functions $f(\tilde{K}_1, K_2) = \frac{\partial e(\tilde{K}_1, K_2)}{\partial \tilde{K}_1} = 0$ and $g(\tilde{K}_1, K_2) = \frac{\partial e(\tilde{K}_1, K_2)}{\partial \tilde{K}_2} = 0$ are sketched in the $K_2 - \tilde{K}_1$ plane. Their intersection identifies the stationary point for error function e, which is also the local minimum in the $K_2 > \tilde{K}_1$ region. In Fig. 6b, c, the error e of Eq. (7) evaluated for points belonging to curve $g(\tilde{K}_1, K_2) = \frac{\partial e(\tilde{K}_1, K_2)}{\partial \tilde{K}_2} = 0$ is represented in the $K_2 - e$ and $\tilde{K}_1 - e$ planes respectively. As can be seen, a quite visible minimum point is present is both cases, which allows a direct evaluation of kinetic constants $\tilde{K}_1$ and K_2.

While in this case (curing temperature equal to 160 °C), such graphical approach is not strictly necessary to find $\tilde{K}_1$ and K_2 values minimizing e, it will be very useful for curing temperatures equal to 180 and 200 °C, where it is found that implicit functions $f(\tilde{K}_1, K_2) = \frac{\partial e(\tilde{K}_1, K_2)}{\partial \tilde{K}_1} = 0$ and $g(\tilde{K}_1, K_2) = \frac{\partial e(\tilde{K}_1, K_2)}{\partial \tilde{K}_2} = 0$ almost coincide.

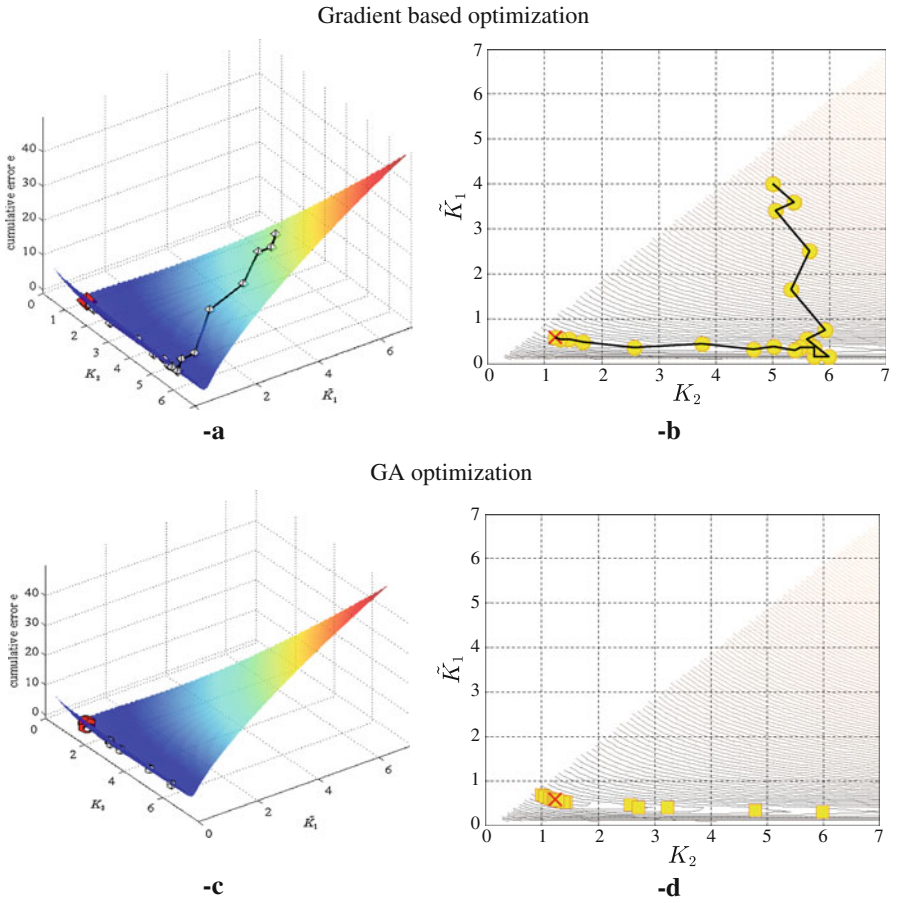

Fig. 3 Experimental data set at 160 °C. Representation of the e error function in the $\tilde{K}_1 - K_2$ domain, and successive optimal points from gradient method (**a**) & (**b**) and GA (**c**) & (**d**)

Finally, in Fig. 6d, a representation of the error e for points belonging to $g(\tilde{K}_1, K_2) = \frac{\partial e(\tilde{K}_1, K_2)}{\partial \tilde{K}_2} = 0$ superimposed to the 3D error e surface is provided, to give a quite direct, albeit approximate, idea of the location of the minimum point.

Comparisons among all models for temperatures equal to 180 and 200 °C are replicated in Figs. 7, 8, 9, 10, 11, 12, 13, and 14, again with a representation of the error functions e and e_2.

In both cases (see Figs. 7, 11 for curing temperatures equal to 180 and 200 °C, respectively), the agreement with the experimental response is very accurate. As can be noted, very few experimental points are needed to obtain quite reliable reproductions of the actual experimental curves.

As expected, reversion is rather marked at 200 °C, but has a perceivable effect also for the cure curve at 180 °C. In both these latter cases, Eq. (6) model progressively

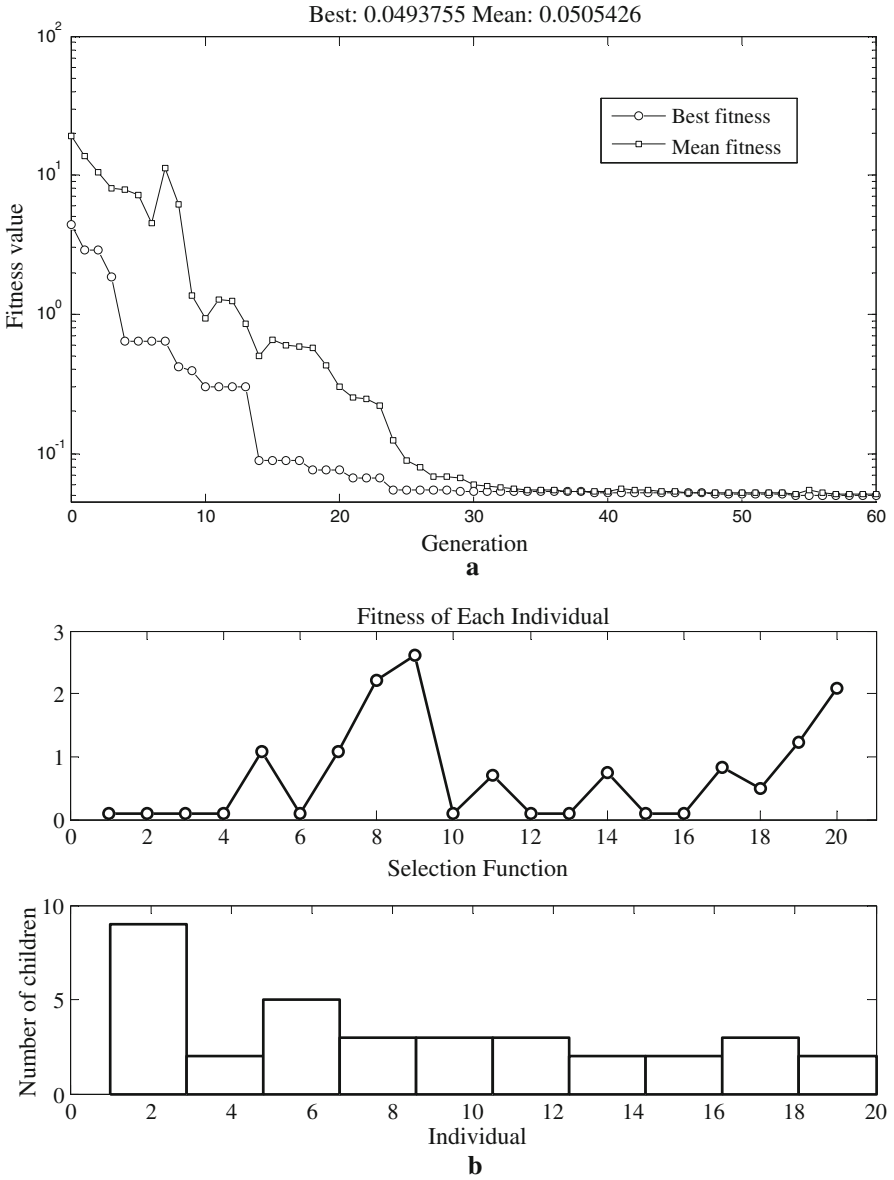

Fig. 4 Experimental data set at 160 °C. Representation of GA best and mean fitness values at successive iterations (**a**) and **b** fitness of each individual at the last generation (60) with the number of children produced

loses accuracy, especially at increasing curing times, being reversion completely disregarded.

In Figs. 8 and 12, the efficiency of the GA approach is compared to the standard gradient method [30] at 180 and 200 °C respectively. As it is possible to notice from the 2D representation of the points with best fitness at successive iterations (Figs. 8d, 12d),

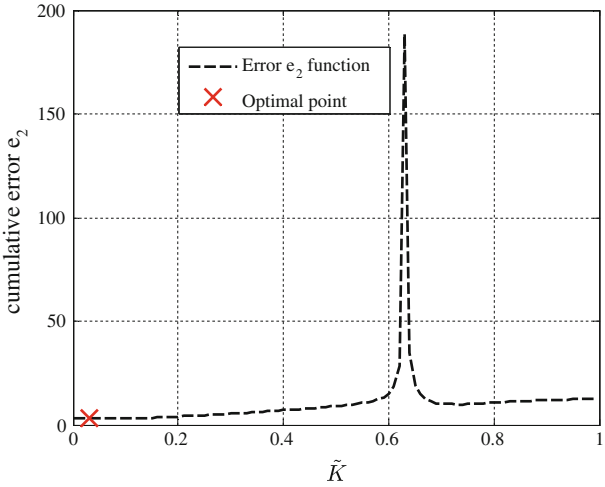

Fig. 5 Experimental data set at 160 °C. Representation of the cumulative e_2 error function in the $\tilde{K}$ domain and optimal point provided either by gradient method or GA

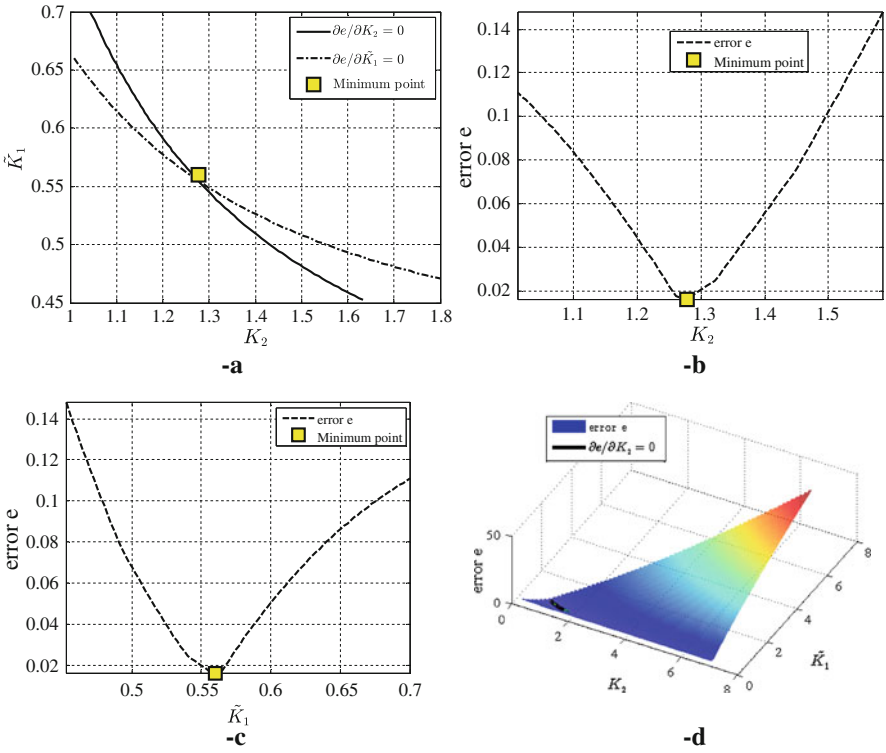

Fig. 6 Experimental data set at 160 °C. **a** $\partial e/\partial \tilde{K}_1 = 0$ and $\partial e/\partial K_2 = 0$ functions. **b** $K_2 - e$ function on $\partial e/\partial K_2 = 0$. **c** $\tilde{K}_1 - e$ function on $\partial e/\partial K_2 = 0$. **d** Representation of $\partial e/\partial K_2 = 0$ on the 3D error function e

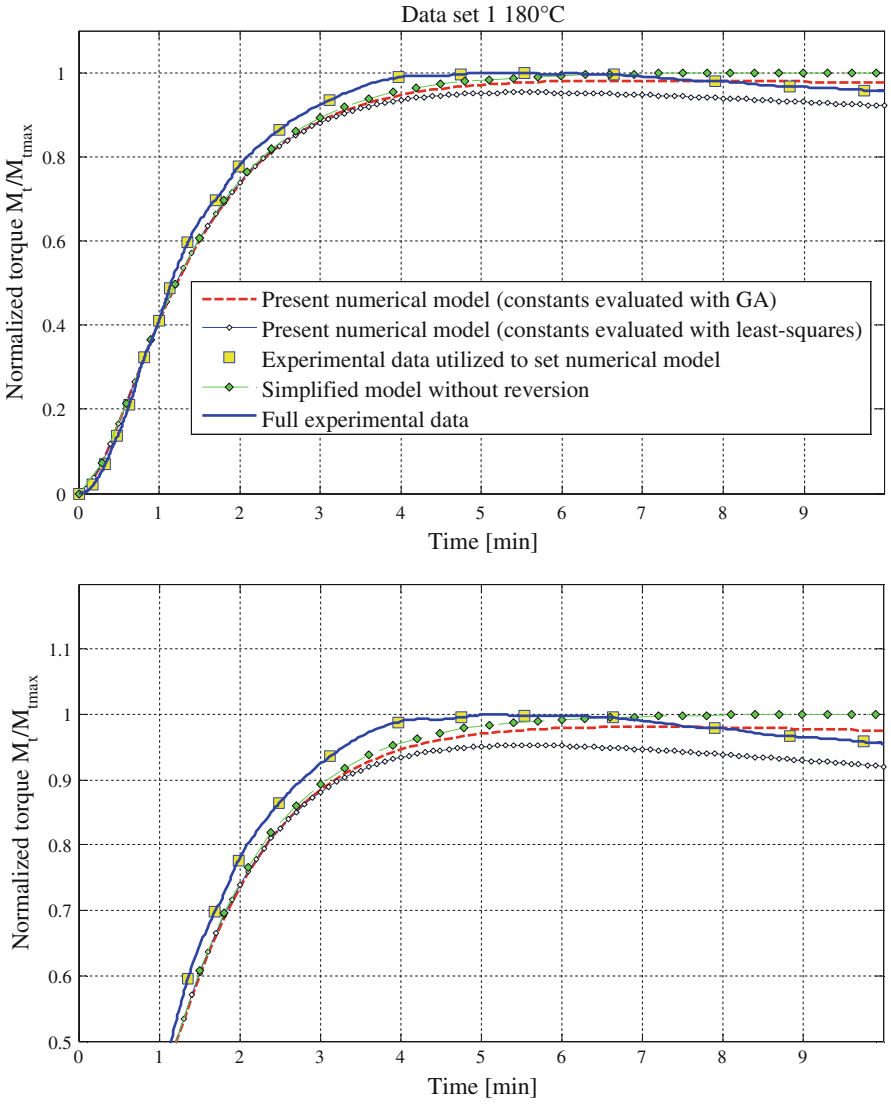

Fig. 7 Experimental data set at 180 °C. Comparison between numerical and experimental curing time-normalized torque (crosslinking density) curves. *Top* entire curve. *Bottom* detail

the number of iterations needed within the GA scheme to obtain solutions near the optimal points is much reduced and clearly smaller than those required by a standard gradient method. Author experienced that the performance of the algorithm seems to increase regularly with curing temperature (compare, for instance Figs. 3, 8, 12).

Constants $\tilde{K}$ at 180 and 200 °C are again evaluated minimizing function e_2. A representation of function e_2 with the indication of the minimum point corresponding

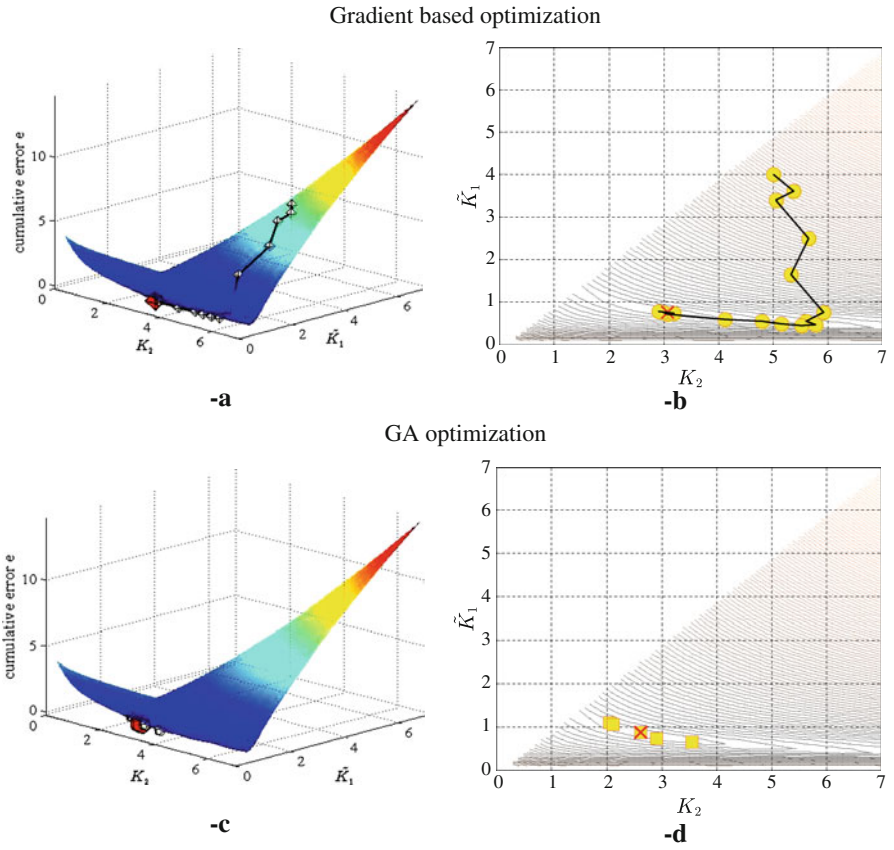

Fig. 8 Experimental data set at 180 °C. Representation of the e error function in the $\tilde{K}_1 - K_2$ domain, and successive optimal points from gradient method (**a**) & (**b**) and GA (**c**) & (**d**)

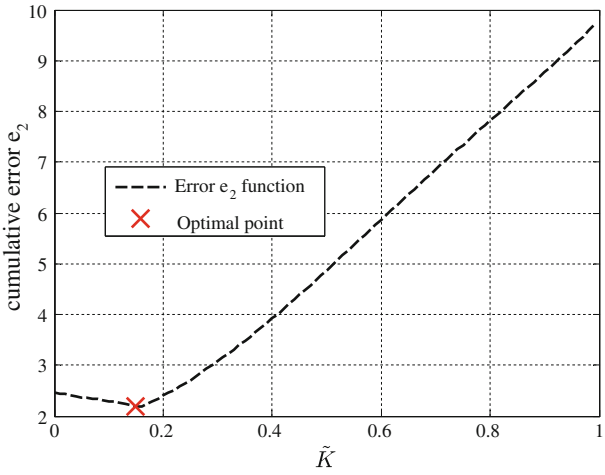

Fig. 9 Experimental data set at 180 °C. Representation of the cumulative e_2 error function in the $\tilde{K}$ domain and optimal point provided either by gradient method or GA

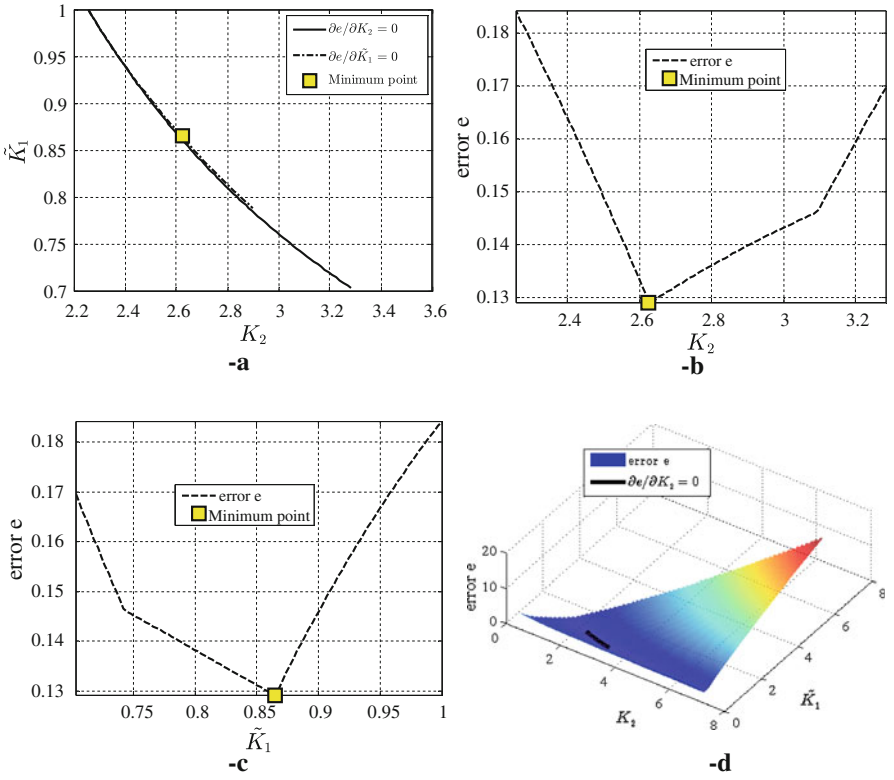

Fig. 10 Experimental data set at 180 °C. **a** $\partial e/\partial \tilde{K}_1 = 0$ and $\partial e/\partial K_2 = 0$ functions. **b** $K_2 - e$ function on $\partial e/\partial K_2 = 0$. **c** $\tilde{K}_1 - e$ function on $\partial e/\partial K_2 = 0$. **d** Representation of $\partial e/\partial K_2 = 0$ on the 3D error function e

to the actual kinetic constant $\tilde{K}$ is provided in Figs. 9 and 13 for temperatures equal to 180 and 200 °C respectively.

Finally in Figs. 10a and 14a, implicit functions $f(\tilde{K}_1, K_2) = \frac{\partial e(\tilde{K}_1, K_2)}{\partial \tilde{K}_1} = 0$ and $g(\tilde{K}_1, K_2) = \frac{\partial e(\tilde{K}_1, K_2)}{\partial \tilde{K}_2} = 0$ are represented. As can be noted, for both cure temperatures (180 and 200 °C) functions f and g almost coincide, making the procedure summarized in Eq. (8) inapplicable in practice. To circumvent this limitation, values of kinematic constants $\tilde{K}_1$ and K_2 which minimize error function e are found with a graphical procedure simply plotting error e for points belonging either to functions f and g in the $K_2 - e$ and $\tilde{K}_1 - e$ planes respectively.

Values of constants $\tilde{K}_1$ and K_2 may be determined either numerically of graphically from Fig. 10b, c at 180 °C and from Fig. 14b, c at 200 °C.

Finally, to have an immediate insight into the approximate position of the local minimum, in Fig. 10d (180 °C) and Fig. 14d (200 °C), error e for points belonging to $g(\tilde{K}_1, K_2) = \frac{\partial e(\tilde{K}_1, K_2)}{\partial \tilde{K}_2} = 0$ is superimposed to the 3D error e surface.

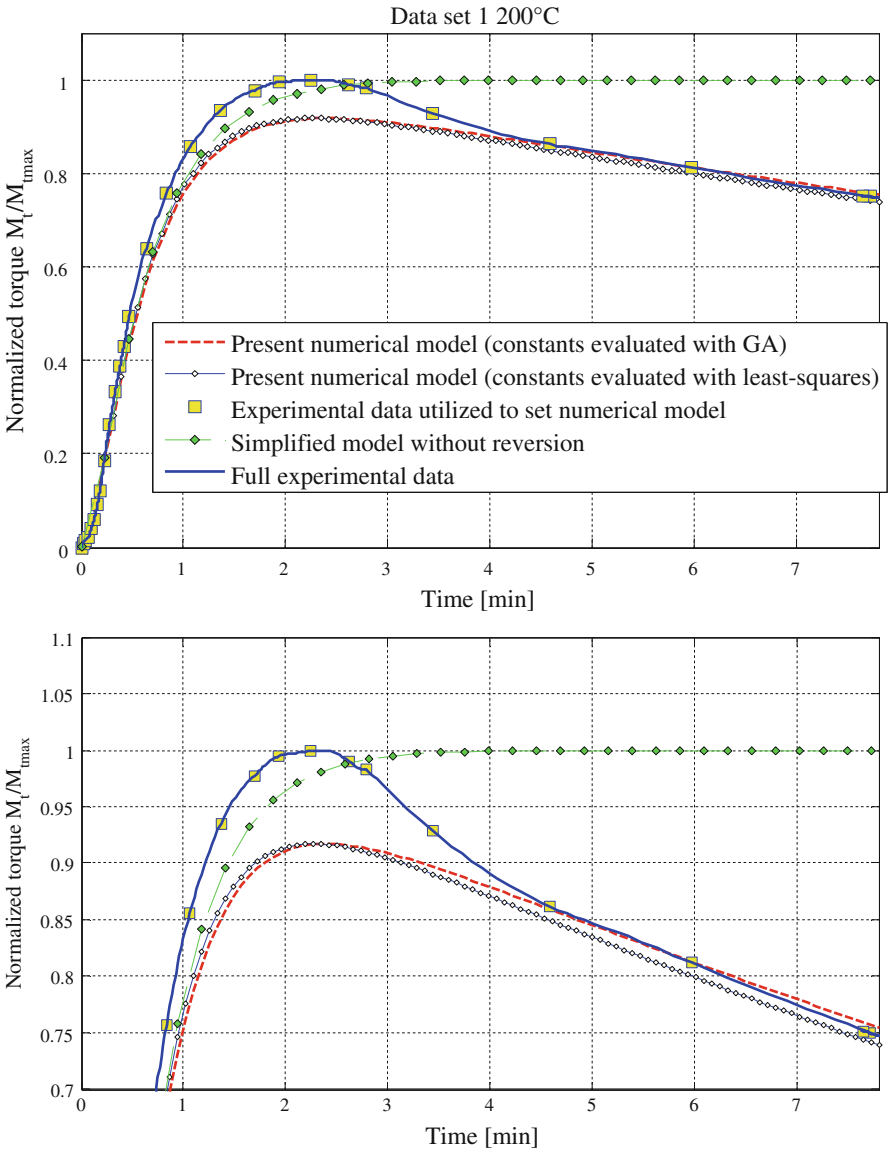

Fig. 11 Experimental data set at 200 °C. Comparison between numerical and experimental curing time-normalized torque (crosslinking density) curves. *Top* entire curve. *Bottom* detail

5 Conclusions

In the present paper, a new GA approach has been utilized to determine reaction kinetic constants within an existing mathematical procedure [14,15], aimed at interpreting EPDM accelerated sulphur curing.

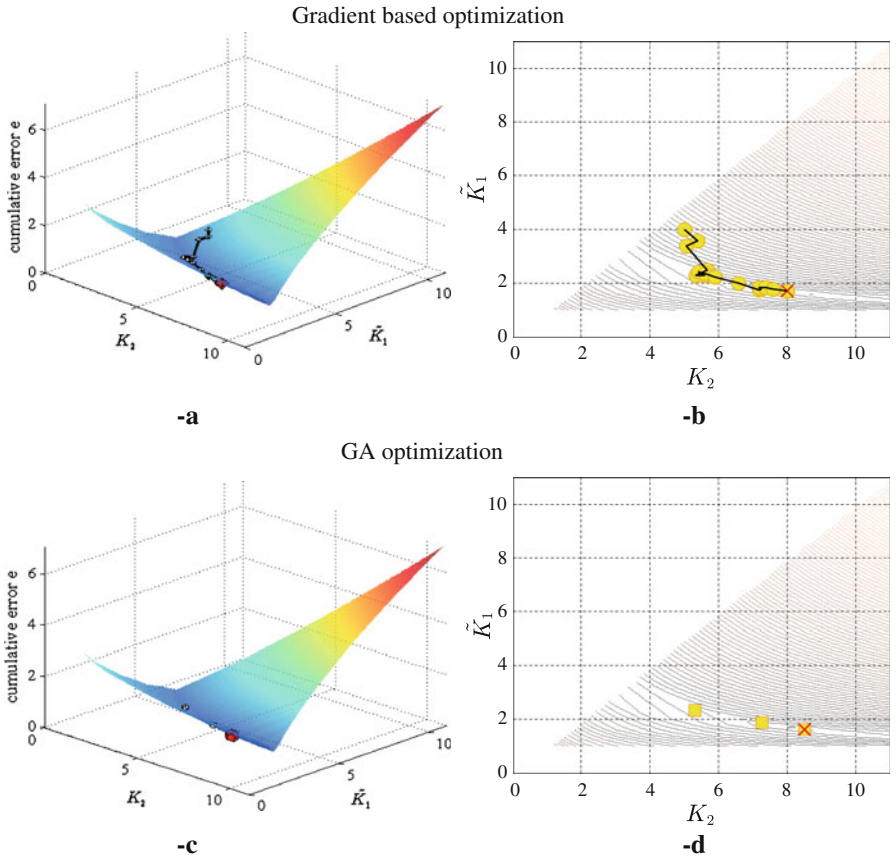

Fig. 12 Experimental data set at 200 °C. Representation of the e error function in the $\tilde{K}_1 - K_2$ domain, and successive optimal points from gradient method (**a**) & (**b**) and GA (**c**) & (**d**)

The existing mathematical model bases on a preliminary characterization of rubber through standard rheometer tests and allows an accurate prediction of the crosslinking degree at both successive curing times and different controlled temperatures.

While in [14,15] a calibration of three kinetic constants at fixed temperature by means of non-linear least-squares fitting was required, the method here proposed circumvents the typical inefficiencies of non-linear data fitting and avoids possible non convergence limitations, disregarding at a first attempt reversion and finding the local minimum of a suitable two-variable error function, to have an estimate of the first two kinetic constants. A comparison between present GA approach and traditional gradient based algorithms has been also discussed, with a substantial reduction of optimization time needed. The last constant, representing reversion has been evaluated through a minimization performed on a single variable error function. The applicability of the approach is immediate and makes the model extremely appealing when fast and reliable estimates of crosslinking density of cured EPDM are required. To show the capabilities of the approach proposed, a comprehensive comparison with both avail-

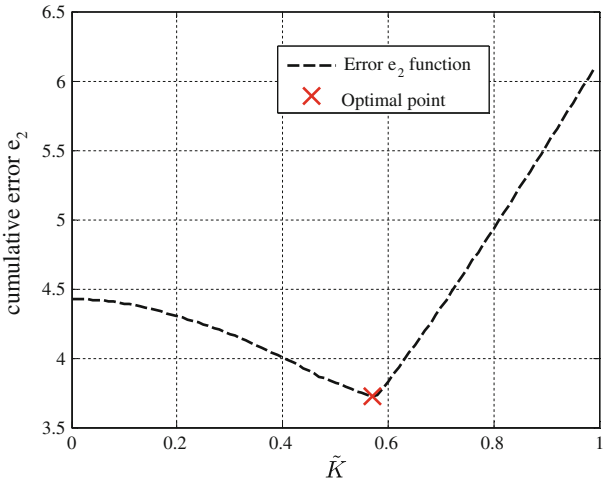

Fig. 13 Experimental data set at 200 °C. Representation of the cumulative e_2 error function in the $\tilde{K}$ domain and optimal point provided either by gradient method or GA

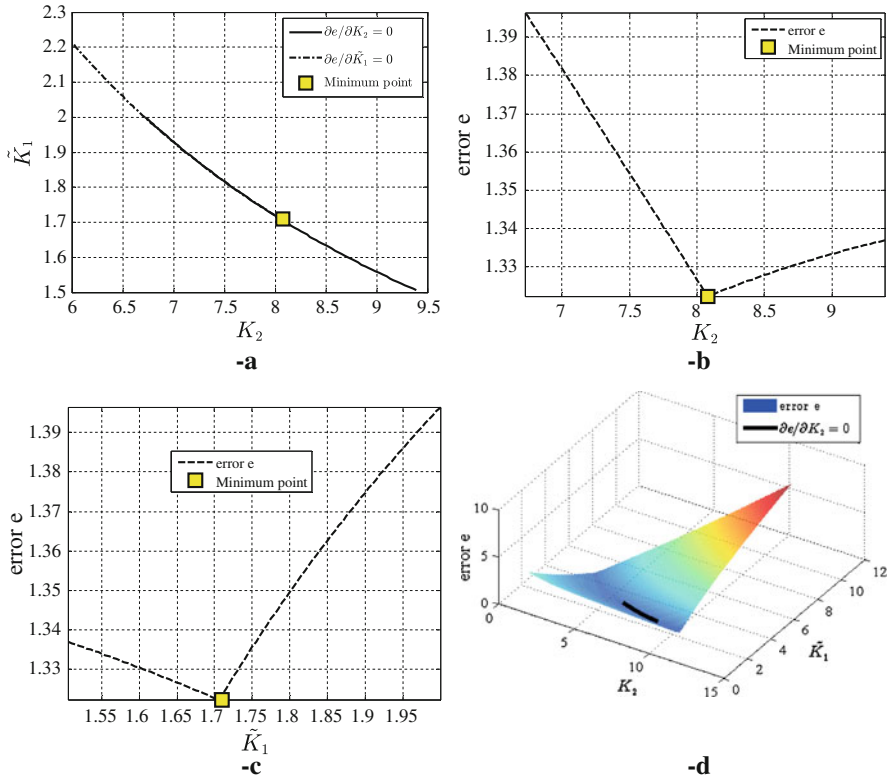

Fig. 14 Experimental data set at 200 °C. **a** $\partial e/\partial \tilde{K}_1 = 0$ and $\partial e/\partial K_2 = 0$ functions. **b** $K_2 - e$ function on $\partial e/\partial K_2 = 0$. **c** $\tilde{K}_1 - e$ function on $\partial e/\partial K_2 = 0$. **d** Representation of $\partial e/\partial K_2 = 0$ on the 3D error function e

able experimental data and results obtained numerically with a least square exponential model for a real compound at different temperatures has been finally provided.

References

1. B. Likozar, Kinetic modeling of the peroxide cross-linking of polymer/monomer blends: from a theoretical model framework to its application for a complex polymer/monomer dispersion system. React. Funct. Polym. **71**(1), 11–22 (2011)
2. B. Likozar, M. Krajnc, Simulation of chemical kinetics of elastomer crosslinking by organic peroxides. Polym. Eng. Sci. **49**(1), 60–72 (2009)
3. E.A. McCaslin, Computer modeling of rubber vulcanization. Rubber World **237**(3), 38–41 (2007)
4. D. Bacci, R. Marchini, M.T. Scrivani, Constitutive equation of peroxide cross-linking of thermoplastic polyolefin rubbers. Polym. Eng. Sci. **45**(3), 333–342 (2005)
5. J.A. Brydson, *Rubbery Materials and Their Compouds* (Elsevier, Amsterdam, 1988)
6. F.W. Billmeier Jr., *Textbook of Polymer Science*, 3rd edn. (Wiley, London, 1984)
7. L. Bateman (ed.), *The Chemistry and Physics of Rubber-Like Substances* (MacLaren, London, 1963)
8. C. Goodyear US Patent 3633 (1844)
9. M. Morton (ed.), *Rubber Technology*, 2nd edn. (Van Nostrand Reinhold, New York, 1981)
10. M.L. Krejsa, J.L. Koenig, Solid state CNMR studies of vulcanized elastomers. XI. N-t-Butyl benzothiazole sulfenimide accelerated sulphur vulcanization of cis-polyisoprene at 75 MHz. Rubber Chem. Technol. **66**, 73–82 (1993)
11. M.L. Krejsa, J.L. Koenig, A review of sulphur cross-linking fundamentals for accelerated and unaccelerated vulcanization. Rubber Chem. Technol. **66**, 376–410 (1993)
12. G. Milani, F. Milani, A new simple numerical model based on experimental scorch curve data fitting for the interpretation of sulphur vulcanization. J. Math. Chem. **48**, 530–557 (2010)
13. G. Milani, F. Milani, A three function numerical model for the prediction of vulcanization-reversion of rubber during sulfur curing. J. Appl. Polym. Sci. **119**, 419–437 (2011)
14. G. Milani, F. Milani, EPDM accelerated sulfur vulcanization: a kinetic model based on a genetic algorithm. J. Math. Chem. **49**(7), 1357–1383 (2011)
15. G. Milani, F. Milani, Simple kinetic numerical model based on rheometer data for Ethylene–Propylene –Diene Monomer accelerated sulfur crosslinking. J. Appl. Polym. Sci. **124**(1), 311–324 (2012)
16. G. Milani, F. Milani, Direct and closed form analytical model for the prediction of reaction kinetic of EPDM accelerated sulphur vulcanization. J. Math. Chem. **50**, 2577–2605 (2012)
17. S.K. Henning, The Use of Coagents in Sulfur Vulcanization: Functional Zinc Salts. in *Proceedings of Spring 167th Technical Meeting of the Rubber Division, American Chemical Society*, San Antonio, TX, May 16–18 (2005)
18. L. Corbelli, S. Codiglia, S. Giovanardi, F. Milani, G.C. Ottavi, R. Zucchini, 36th Report Montedison to B.F. Goodrich, May (1977)
19. J.S. Dick, H. Pawlowski, Alternate instrumental methods of measuring scorch and cure characteristics. Polym. Test. **14**, 45–84 (1995)
20. B.T. Poh, K.W. Wong, Effect of blend ratio on Mooney scorch time of rubber blends. J. Appl. Polym. Sci. **69**, 1301–1305 (1998)
21. B.T. Poh, C.C. Ng, Effect of silane coupling agents on the Mooney scorch time of silica-filled natural rubber compound. Eur. Polym. J. **34**, 975–979 (1998)
22. B.T. Poh, M.F. Chen, B.S. Ding, Cure characteristics of unaccelerated sulfur vulcanization of epoxidized natural rubber. J. Appl. Polym. Sci. **60**, 1569–1574 (1996)
23. B.T. Poh, E.K. Tan, Mooney scorch time and cure index of epoxidized natural rubber in presence of sodium carbonate. J. Appl. Polym. Sci. **82**, 1352–1355 (2001)
24. B.T. Poh, H. Ismail, K.S. Tan, Effect of filler loading on tensile and tear properties of SMR L/ENR 25 and SMR L / SBR blends cured via a semi-efficient vulcanization system. Polym. Test. **21**, 801–806 (2002)
25. C.H. Chen, E.A. Collins, J.R. Shelton, J.L. Koenigs, Compounding variables influencing the reversion process in accelerated curing of natural rubber. Rubber Chem. Tech. **55**(4), 1221–1232 (1982)
26. C.T. Loo, High temperature vulcanization of elastomers: 2. Network structures in conventional sulphenamide-sulphur natural rubber vulcanizates. Polymer **15**(6), 357–365 (1974)

27. N.J. Morrison, M. Porter, in *Crosslinking of Rubbers*, ed. by G. Allen The Synthesis, Characterization, Reactions and Applications of Polymers (Pergamon press, Oxford, 1984)
28. G. Evans, J. Blackledge, P. Yardley, *Numerical Methods for Partial Differential Equations*, 2nd edn. (Springer, Berlin, 2001)
29. T.F. Coleman, Y. Li, Math. Program. **67**(2), 189–224 (1994)
30. R. Fletcher, *Practical Methods of Optimization,* vol 1*, Unconstrained Optimization* (Wiley, London, 1980)
31. D.E. Goldberg, *Genetic Algorithms in Search, Optimization and Machine Learning* (Addison Wesley, Reading, 1989)
32. R.B. Holstien, Artificial genetic adaptation in computer control systems. Ph.D. Thesis, Department of Computer and Communication Sciences, University of Michigan, Ann Arbor (1971)
33. R.L. Haupt, S.E. Haupt, *Practical Genetic Algorithms* (Wiley, London, 2004)
34. R. Ding, I. Leonov, A kinetic model for sulfur accelerated vulcanization of a natural rubber compound. J. Appl. Polym. Sci. **61**, 455–463 (1996)
35. R. Ding, I. Leonov, A.Y. Coran, Study of the Vulcanization Kinetics of an Accelerated-Sulfur SBR Compound. Rubber Chem. Technol. **69**, 81 (1996)
36. V. Duchacek, M. Duskova, Cure curve with two plateaus—the result of individual vulcanization reactions. J. Polym. Eng. **21**, 341 (2001)
37. M.R. Kamal, S. Sourour, Kinetics and thermal characterization of thermoset cure. Polym. Eng. Sci. **13**, 59 (1973)
38. A. Arrillaga, A.M. Zaldua, R.M. Atxurra, A.S. Farid, Techniques used for determining cure kinetics of rubber compounds. Eur. Polym. J. **43**, 4783–4799 (2007)
39. A.Y. Coran, Vulcanization, chap. 7, in *Science and Technology of Rubber*, ed. by J.E. Mark, B. Erman, F.R. Eirich. (Academic Press, New York, 1978)
40. M. van Duin, Kaut. Gummi Kunststoffe, 55 Jarghang, 2 (2002)
41. G. Milani, F. Milani, Genetic Algorithm for the determination of binodal curves in ternary systems Polymer/Liquid(1)/Liquid(2) and Polymer(1)/Polymer(2)/Solvent. J. Comput. Chem. **28**(13), 2203–2215 (2007)